Strand switching mechanism of Pif1 helicase induced by its collision with a G-quadruplex embedded in dsDNA

Jessica Valle-Orero [1,2,*], **Martin Rieu**[1,2], **Phong Lan Thao Tran**[3], **Alexandra Joubert**[3], **Saurabh Raj**[1], **Jean-François Allemand**[1,2], **Vincent Croquette**[1,2,4,*] and **Jean-Baptiste Boulé** [3,*]

[1]Laboratoire de physique de L'École Normale Supérieure de Paris, CNRS, ENS, Université PSL, Sorbonne Université, Université Paris Cité, 75005 Paris, France, [2]Institut de Biologie de l'École Normale Supérieure de Paris (IBENS), École Normale Supérieure, CNRS, INSERM, Université PSL, 75005 Paris, France, [3]Structure et Instabilité des Génomes, Museum National d'Histoire Naturelle, INSERM, CNRS, Alliance Sorbonne Université, 75005 Paris, France and [4]ESPCI Paris, Université PSL, 75005 Paris, France

ABSTRACT

G-rich sequences found at multiple sites throughout all genomes may form secondary structures called G-quadruplexes (G4), which act as roadblocks for molecular motors. Among the enzymes thought to process these structures, the Pif1 DNA helicase is considered as an archetypical G4-resolvase and its absence has been linked to G4-related genomic instabilities in yeast. Here we developed a single-molecule assay to observe Pif1 opening a DNA duplex and resolving the G4 in real time. In support of former enzymological studies, we show that the helicase reduces the lifetime of G4 from hours to seconds. However, we observe that in the presence of a G4, Pif1 exhibits a strong strand switching behavior, which can lead to Pif1 escaping G4 resolution, depending on the structural context surrounding the substrate. This behavior is also detected in the presence of other roadblocks (LNA or RNA). We propose that the efficiency of Pif1 to remove a roadblock (G4 or other) is affected by its strand switching behavior and depends on the context surrounding the obstacle. We discuss how this switching behavior may explain several aspects of Pif1 substrate preference and affect its activity as a G4 resolvase *in vivo*.

GRAPHICAL ABSTRACT
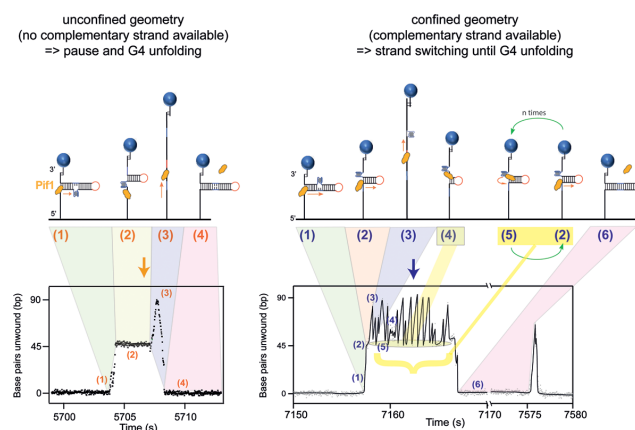
INTRODUCTION

G-quadruplexes (G4) are nucleic acids (NA) secondary structures that may form when four stretches of successive guanines appear consecutively along the primary sequence. Under appropriate ionic conditions, guanines of each stretch line up to form planes (G-quartets) with four coplanar guanines interacting via Hoogsteen hydrogen bonds. Between these planes, cations such as K^+ help stabilize the structure, which may form intra- or intermolecularly and have different folding patterns (typically referred to as parallel, antiparallel or mixed structures (1,2)). Formation

of nucleic acids such as G4 are suspected of acting as road-blocks for the replication machinery, causing fork pausing and potentially promoting DNA breakage (3–6). Despite causing potential roadblocks for molecular motors, there is increasing evidence that many G4 forming sequences were selected during evolution, suggesting a role for encoding structural information within DNA at the expense of evolving protein motors able to remove these stable structures during DNA replication or repair (7–10). A well-studied G4-resolving motor is the *Saccharomyces cerevisiae* DNA helicase Pif1, a multifunctional helicase which plays multiple roles in nuclear and mitochondrial genome stability, including resolution of G4 structures (11). Pif1 exhibits a 5′-to-3′ polarity and translocates on ssDNA while displacing complementary DNA, RNA or proteins (12–15). Both bulk and single molecule studies have shown that Pif1 has a high affinity for DNA but unwinds double-stranded DNA (ds-DNA) with low processivity (14,16,17) and that dimerization of Pif1 is necessary for efficient translocation on DNA (18,19). In addition, single molecule studies have led to the proposition of a mechanism named 'patrolling', which consists of Pif1 reeling ssDNA while anchored at a ss-dsDNA junction (16). In a separate study, however, this activity was shown to be rare compared to translocation (20).

Interestingly, repetitive unwinding of a substrate by Pif1 has been a regular theme in Pif1 single molecule studies, but the underlying mechanism has remained unclear (21). Therefore, a complete description of Pif1 translocation mechanism, its substrate preference and its mechanism of G4 unwinding is still lacking. A main experimental challenge for studying intramolecular G4 unwinding in single molecule assays is to be able to control the formation and lifetime of G4 structures. We recently developed a single molecule assay (22) allowing embedding a G4 structure within a dsDNA molecule, mimicking a dsDNA fork, a situation which may occur in the cell during replication or at a gene promoter. Using this assay, we aim to gain insights into the mechanism of G4 resolution by the *Saccharomyces cerevisie* Pif1. Here, we provide a real-time visualization of Pif1 translocating along dsDNA and interacting with G4 structures taken from the promoter of the human c-MYC gene. We monitored the position of the fork with a resolution of a few nanometers, allowing us to follow the helicase at a few base pairs resolution as it encounters the embedded G4. We show that in the presence of an available single-stranded DNA (ssDNA) in the vicinity of the enzyme upon collision with the G4, Pif1 exhibits a strand switching behavior. In this situation, G4 resolution depends therefore on the ability of Pif1 to collide multiple times with the G4 after several rounds of strand switching. In the absence of a ssDNA strand in the vicinity of the enzyme, the enzyme pauses in front of the obstacle until it removes the G4 and resumes translocation. Finally, we show that Pif1 exhibits strand switching in the presence of other obstacles, namely LNA:DNA or RNA:DNA hybrids and obtained the probability rate of this mechanism for each substrate; we also validated this strand switching behavior for another G4 structure, namely a replication origin from the chicken genome (β^A-ori (23)). Our results suggest that the ability of Pif1 to remove a G4 (or other obstacles) is affected by the availability of a ssDNA allowing strand switching. We discuss the relevance of our observations in the context of Pif1 substrate preference and *in vivo* roles.

MATERIALS AND METHODS

DNA substrate

All oligonucleotides were bought from Eurogentec (Seraing, Belgium) or Integrated DNA Technologies (Leuven, Belgium). The tethered DNA substrate was a 310-bases long molecule comprised of a 87-bp hairpin region, a 6-nucleotide loop, and two ssDNA handles allowing attachment to the surface and the magnetic bead respectively. We designed two versions of the substrate that differ in the way Pif1 encounters the G4: one where the G4 collision occurs when opening the hairpin (*LagG4*) and one where Pif1 collides with the G4 while the hairpin is closing behind the translocating helicase (*LeadG4*). *LagG4* contains the c-MYC-Pu27 G4-motif (GGG-GAG-GGT-GGG-GAG-GGT-GGG-GAA-GG) in the center of the hairpin region, between the 5′ extremity and the loop. *LeadG4* contains the same motif, this time between the loop and the 3′ extremity. Both hairpins are formed via ligation of three oligonucleotides, Oligo5$_X$, Oligo3$_X$ and OliLoop, where X stands for *LeadG4* or *LagG4*. The 5′ ss-handle of the hairpins is complementary to a 58-base 3′-DBCO modified oligonucleotide (OliD-BCO) attached to the surface. The 3′-end of the hairpin is complementary to a 57-base oligonucleotide (OliBiotin), which contains two biotin modifications at its 5′-end. Between the region complementary to OliDBCO and the hairpin region, seven bases (poly-dT) of ssDNA allow the binding of Pif1 to the substrate. A schematic of the single-molecule substrate is available on Supplementary Figure S1. Besides c-MYC-Pu27, we built another *LeadG4* assay that contains the sequence of a less stable G4 structure called β^A-ori. It is known to form in a replication origin found in the chicken genome (GGGGGGGGGGGGGGGCGGG) (see Suplementary Information) (22,23).

OliRNA and OliLNA are 34-bases oligonucleotides that are complementary to the *LeadG4* hairpin region containing the G4 motif. OliLNA is composed of 25 bases of DNA and 9 bases of LNA on its 3′ extremity. All oligonucleotide sequences are available in Supplementary Tables S1 and S2.

Magnetic tweezers

All our measurements were carried out using magnetic tweezers, which is a single-molecule force spectroscopy technique (24). They allow measuring extensions of single DNA hairpin molecules tethered to a surface on one end and on a magnetic bead on the other end, while a force is applied through a magnetic bead. The force is provided by a couple of permanent magnets and is proportional to the magnetic field gradient (25–28). The force is calibrated using the fluctuation dissipation theorem and can be modified by changing the distance of the magnets to the surface. Our force range expands from 0 to 22 pN, with a variability from bead to bead of 10%, due to the heterogeneity of their magnetization. The magnets are positioned with a DC-motor (Physik Instrumente, M-126-PD) to modulate the force. Up to 100 magnetic beads are imaged using a CMOS camera.

Their 3D-position is inferred in real-time with a resolution of a few nanometers using tracking techniques.

Bead preparation

The purified DNA hairpin was first hybridized with OliBiotin during 30 min by mixing both molecules at a final concentration of 5 nM in passivation buffer (140 mM NaCl, BSA 1%, Pluronic F-127 1%, 5 mM EDTA, 10 mM NaN$_3$, pH 7.4). 5 μl of streptavidin coated Dynabeads MyOne T1 (Thermofisher) were washed three times with 200 μl passivation buffer. The hybridized substrate was diluted to 200 pM and 2 μl of this solution was then incubated for 10 minutes with the beads in a total volume of 20 μl of passivation buffer. The beads were then rinsed three times with passivation buffer in order to remove unbound DNA. All the reactions were performed at room temperature.

Pif1 helicase expression and purification

The sequence coding for the nuclear form of *Sacharomyces cerevisiae* Pif1 (amino acids 40–859, in this work referred to as Pif1) fused at its N-terminus to a 6-histidine tag was cloned into vector pET28 (Novagen) and transformed into *Escherichia coli* BL21(DE3) strain (Novagen). Pif1 expression and purification procedure was adapted from (29). Briefly, cells were cultivated in Luria Broth media and protein expression was induced for 16h at 18°C by addition of 0.2 mM IPTG at 0.8 OD$_{600}$, followed by another induction with 0.2 mM IPTG for 4h at the same temperature. The cell pellet was resuspended in buffer P (20 mM sodium phosphate buffer pH 7.5, 500 mM NaCl, 1 mM TCEP and 10% glycerol) and sonicated on ice (40% amplitude, pulse 40%, 10 min, 2 s on/2 s off) to lyse the cells. The lysate was subjected to ultracentrifugation at 30 000g for 1h. The supernatant was applied onto a HisTrap Crude affinity column (Cytiva), washed with five bed volumes of buffer containing 20 mM imidazole and eluted with a 20–200 mM imidazole gradient. Fractions containing Pif1 were loaded onto a CHT column (Biorad) and eluted with a 20–200 mM phosphate gradient. Finally, the fractions containing Pif1 were dialyzed against buffer S (50 mM HEPES pH 7.5, 100 mM KCl, 1 mM TCEP, 10% glycerol), loaded onto a strong cation exchange column (MonoS, Cytiva) and eluted with a 100 mM to 1 M salt gradient. Fractions were separated by electrophoresis on denaturing polyacrylamide gels. Fractions containing pure Pif1 as assessed by Coomassie staining of the gels were pooled, concentrated and stored at –80°C in 25 mM HEPES pH 7.5, 250 mM KCl, 0.5 mM TCEP, 50% glycerol.

Single-molecule Pif1 measurements

Our experiments began with the preparation of a microfluidic chamber coated with OliDBCO (Supplementary Table S2). A 40-μl droplet containing 100 nM OliDBCO and 500 mM NaCl was incubated for two hours on an azide-functionalized coverslip (PolyAn, Berlin, Germany) at room temperature. The coverslips were then rinsed with passivation buffer and assembled into a 10-μl microfluidic chamber. After the chamber was attached to the mag-

netic tweezer setup, 1 μl of the bead solution was introduced into the cell, filled with passivation buffer and incubated for 10 minutes. Excess unbound beads were washed out by flowing passivation buffer into the cell. Measurements started by applying repetitive force cycles between 4 and 19 pN to the tethered molecules. Only molecules that showed an instantaneous unzipping at 19 pN (corresponding to an immediate increase of extension of 100–120 nm), followed by a complete rezipping when the force was lowered to 4 pN, were kept. This signature allowed us to select molecules attached as expected as a result of annealing between OliDBCO and the hairpin molecule, and not through non-specific interactions. Once the well-attached hairpins were identified, the microfluidic chamber was equilibrated with 200 μl G4Pif1 buffer (10 mM Tris–HCl (pH 7.5), 100 mM KCl, 3 mM MgCl$_2$), where potassium enhances the stability of G4 structures and magnesium is necessary for Pif1 activity (30). Then, a 7-base oligonucleotide (Oli7) at a concentration of 10 nM, complementary to the hairpin loop was injected in the solution (Supplementary Table S1). We then repetitively applied the following force cycle: 19 pN for 8s (hairpin unzipping and Oli7 hybridization), 7 pN for 15s (hairpin rezipping blocked by Oli7), and 5 s at 4 pN (expulsion of Oli7 and full rezipping). At 19 pN, the hairpin fully unzips, and rezips at 7 pN. However, the hybridization of Oli7 to the loop at 19 pN temporarily prevents the closing of the hairpin, even at 7 pN. This low force regime with extended ssDNA thanks to Oli7 enables the formation of the G4 structure. This is probed, under the absence of Oli7, as a rezipping of only half of the hairpin (blockage at G4 position) when the force is lowered to 7 pN. See a detailed description of the protocol of G4 formation and detection in (22). Once all G4 were formed and before injecting Pif1, we performed the following force cycle protocol: we increased the force to 19 pN for a full opening of the hairpin, followed by a closing at 7 pN, where again a blockage at the G4 position was observed. We then increased the force to 11 pN for a few seconds to determine the extension of the partially closed hairpin and thus the position of the G4, lowered the force to 4 pN in order to close the hairpin around the G4 (embedded G4) and finally we increased the force to 11 pN (Figure 1B, red). From this point on in the experiment, the force was kept at 11 pN and Pif1 was added to the microfluidic chamber at a concentration of 6 nM and 1 mM ATP lithium salt (Roche) in G4-Pif1 buffer. A flow of 5 μl/min of this Pif1/ATP mix was kept constant throughout the experiments. In the case of the experiments with RNA:DNA and LNA:DNA, the addition of Oli7 was omitted so that G4 folding was not induced (and never observed in our experiments). The same force protocol as above was applied until the hybridization of OliRNA and OliLNA took place, which was observed as the rezipping of only half of the hairpin at 7 pN (same position as the G4).

Data collection and analysis

Molecule extensions and forces were collected in real-time using Xvin, an interactive data visualization software developed in-house in C/C++ (https://tig.phys.ens.fr/ABCDLab/xvin/xvin), at an acquisition frequency of 50 Hz
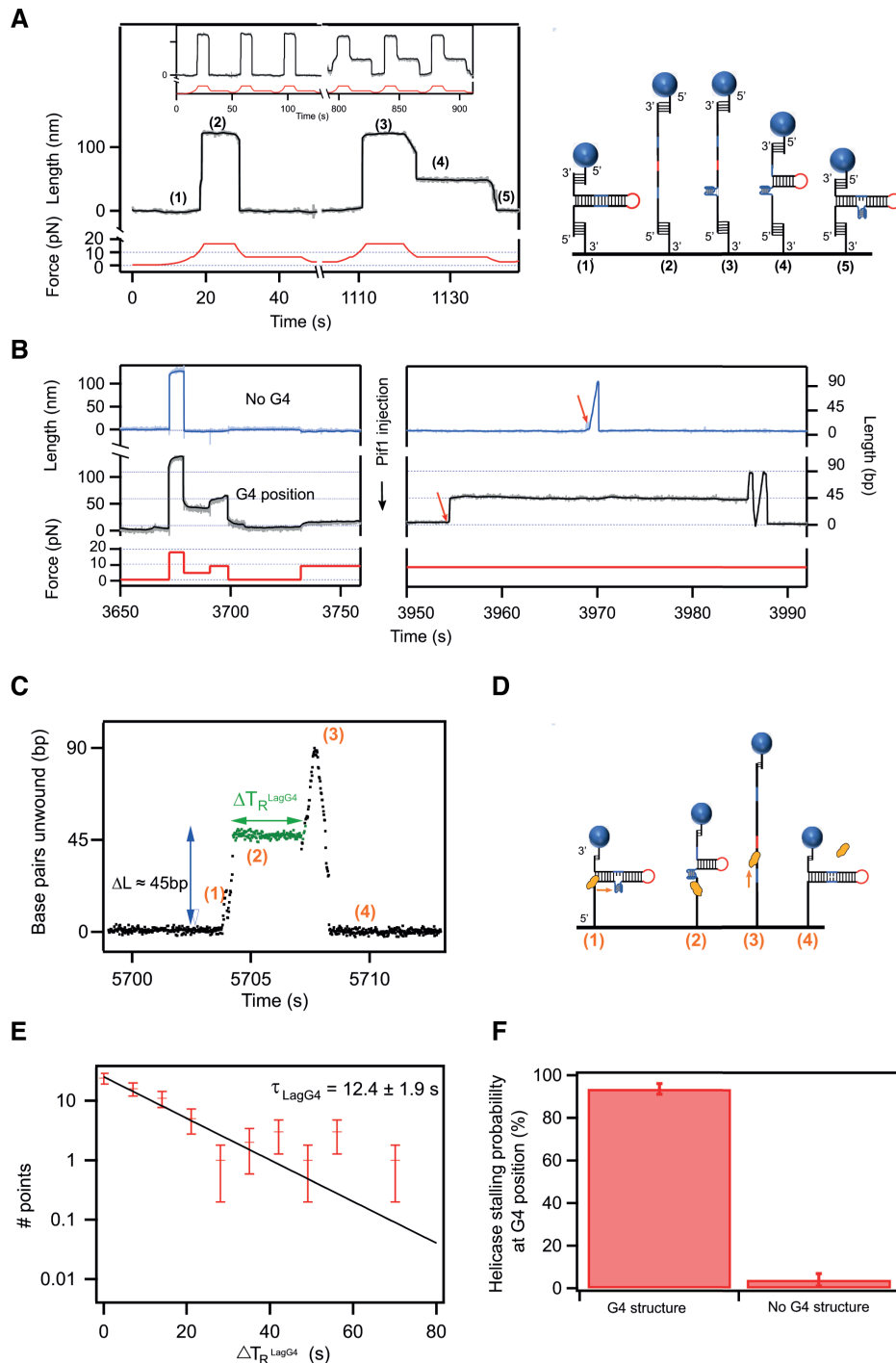
Figure 1. G4 formation and resolution on a *LagG4* hairpin assay. (**A**) G4 prevents the rezipping of the hairpin. Force-extension curves and sketches of our hairpin assay. Force cycles of 19 and 7 pN show unzipping (2) and rezipping (1) of the hairpin respectively. When G4 (represented as a blue tetrad) is formed, a partial rezipping is observed at 7 pN (4); lowering the force even more (4 pN) forces the hairpin to close while encircling the G4 structure (5). (**B**) Pif1 binds to the *LagG4* hairpin. Red trace: Force protocol to test G4 presence and interaction with Pif1. The force is kept constant at 11 pN when Pif1 is injected and throughout the measurement. Blue trace: G4 has not formed, as observed by the lack of blockage when the force is lowered to 7 pN. Pif1 binds to the DNA (red arrow) and translocates throughout the hairpin. Black trace: G4 has formed, as observed by a blockage at 7 pN. Pif1 attaches to the hairpin (red arrow) and unwinds it until it is stalled at the G4 position. (**C**) Pif1 is stalled by the G4. Pif1 opens 30 bp and translocates within the G4 motif for about 15 additional nucleotides (accounting for 45 bp unwound), until it gets stalled by the G4 for a period of time ΔT_R^{LagG4} (green trace, steps 1–2), needed for Pif1 to resolve the G4. As Pif1 continues travelling on the opposite strand (step 3), the hairpin closes back behind the helicase (step 4). (**D**) Sketch of the *LagG4* hairpin showing the extension of the hairpin throughout the different steps from (**C**) as Pif1 (represented as a yellow ellipse) travels through it. (**E**)) Distribution of G4 resolving times. The resolving times show a single exponential distribution characterized by a time constant $\tau_{LagG4} = 12.4 \pm 1.9$ s. (**F**)) Statistics of blockage. Left bar: probability of Pif1 stalling at a G4. Right Bar: Probability of a blockage at the G4 position when a G4 was not present in the previous cycles.

Table 1. Summary of statistics for Pif1 helicase during its interaction with single-molecule substrates

Substrate	Number of molecules	Resolving time τ_x (s) ([Pif1])	Stalling time τ'_x (s)	Stalling position (bp)	v_{unz} (bp/s)	vz (bp/s)
LagG4	71	12.4 ± 1.9	NA	46.3 ± 3.3	108.4 ± 18.2 *95.0 ± 20.1	NA
LeadG4	93	7.1 ± 0.9	0.58 ± 0.06	49.4 ± 4.8	94.6 ± 10.0	113.1 ± 16.0
LagG4 (60 nM)	60	14.6 ± 3.1	NA	NA	NA	NA
LeadG4 (60 nM)	57	5.9 ± 1.0	0.51 ± 0.07	NA	NA	NA
LNA:DNA	115	$\overline{T_{\mathrm{LNA}}}$= 31.1 ± 5.0	0.29 ± 0.03	54.3 ± 5.6	108.2 ± 25.2	108.6 ± 20.8
RNA:DNA	29	$\overline{T_{\mathrm{RNA}}}$=2.2 ± 0.4	0.26 ± 0.02	50.7 ± 3.9	113.4 ± 21.9	86.8 ± 32.7

Table 1 provides the characteristic time rates τ_x and τ'_x obtained from exponential fits of the resolving times and stalling times respectively, for x being any of our substrates: *LagG4, LeadG4, RNA:DNA, LNA:DNA*. Here, v_{unz}: speed of Pif1 in the unzipping phase, and vz: speed of Pif1 in the rezipping phase. The (*) corresponds to the speed of the helicase after resolving a G4 in the *LagG4*. While experiments were carried out at a concentration of ∼6 nM Pif1 helicase, we also took measurements at a higher concentration of 60 nM, as indicated within brackets. Errors on the times are derived from the fitting procedure. Errors on the speeds correspond to the standard deviations of the underlying distributions.

and at a constant temperature of 25°C. Extension graphs were generated using IgorPro (Wavemetrics, Lake Oswego, OR, USA). To interpret the extension of the hairpins as positions of the helicase along the sequence, extensions in nanometers were converted to base pairs. To do so, the average extension change of the hairpins upon unwinding is measured at 11 pN as the distance between the lowest point and the highest point of a full unwinding event of the hairpin by Pif1. This distance is divided by 90 bp (length of the hairpin + loop), which gives the length corresponding to the unwinding of one base pair (see Supplementary Methods). All traces show both the raw data of extension (in nm or bp) versus time (in seconds) (light points) and the filtered data (dark curve). The latter was obtained using a non-linear filter slope algorithm (31).

Individual stalling events during hairpin unwinding and rezipping were manually detected using Xvin. We considered that there was a pause in either unwinding or rezipping when the position of the bead stayed within a window of 5 nm during a time larger than 0.3 s. In comparison, the bead moved at a velocity of ≃ 100 nm/s upon enzyme translocation, and thus would cross a 10-nm window in 0.1 s. Empirically, all stalling events occurred close to the G4 position in the sequence (50 ±5 bases) (see Supplementary Methods). Stalling times $\Delta t'$ correspond to the times elapsed between the start and the end of individual stalling events. The resolving times $\Delta T_R^{xG4} = \Sigma \Delta t'$ (with x being *Lead* or *Lag* substrates) correspond to the total time spent in stalling events by the enzyme before it bypasses the G4 position (stalling position). Between 50 and 100 resolving times were measured for both of the substrates, and histograms were computed with a binsize of around 7 s. The histograms and corresponding errors ($\sqrt{N}$, N being the frequency in each bin) were fitted to single exponential distributions using IgorPro. The characteristic time rates τ_{LagG4} and τ_{LeadG4} and their errors correspond to the parameters inferred from this fitting procedure.

In our studies of Pif1 with LNA:DNA and RNA:DNA heteroduplexes, we computed the resolving times as the average of the contact times of Pif1 with the heteroduplexes before the removal of the oligonucleotide, defined as $\overline{T_{\mathrm{LNA}}}$ and $\overline{T_{\mathrm{RNA}}}$ for LNA and RNA respectively. Likewise, we also obtained $\Delta t'$. The histograms of $\Delta t'$ were computed with a binsize of 0.2 or 0.3 s, and fitted to single exponential dis-

tributions, from which a time constant τ'_x (where x stands for G4, LNA or RNA) was obtained. Note that both the stalling time and the resolving time are two independent events, each following an exponential distribution (Supplementary Figure S2).

Translocation velocities of Pif1 were measured separately during hairpin unzipping (v_{unz}) and rezipping (v_z) for all our substrates by fitting the position of the bead with a linear function. More than 50 slopes from individual events obtained this way were then averaged to obtain the mean translocation velocities. Average velocities were converted from nm/s to bp/s as explained in Supplementary Methods. All these statistics are summarized in Table 1 and in Supplementary Table S3.

RESULTS

Single-molecule observation of Pif1 unwinding a G4-containing hairpin unveils how it resolves the secondary structure

We investigated the interaction between Pif1 and a G-quadruplex structure while the helicase unwinds dsDNA. For this purpose, we designed a hairpin of 87 base pairs which sequence contains the G4 motif of the c-Myc promoter sequence (c-Myc Pu27) (32) (see Supplementary Figure S1).

Formation and detection of a G4 embedded in a dsDNA. We formed the G4 structure in the lagging strand of a hairpin (*LagG4*) by applying repetitive force cycles in the presence of 100 mM potassium and of a 7 nt oligonucleotide complementary to the hairpin apex. In order to form the G4 structure in the hairpin, we first need to convert the hairpin in a ssDNA structure, and we do so by opening the hairpin at a force higher than 15 pN. However at this force the G4 formation is very slow (folding time increases with increased force). Thus, we add the 7 nt oligonucleotide which hybridizes in the hairpin apex to transiently prevent the closure of the hairpin at low force, therefore allowing the folding of the G4 structure. This method used to preform the G4 structure before injecting Pif1 is described in detailed in (22).

Figure 1A shows the changes of extension of the hairpin upon changes in the pulling force. Pulling on a closed hair-

pin (step-(1)) at 19 pN results in its full unzipping and consequent increase of the extension by about 120 nm (∼90 bp) (step-(2)). When the force is lowered to 7 pN, the hairpin rezips (back to step-(1)). However, when G4 forms, the opened hairpin (step-(3)) only partially closes back (step-(4)) when the force is reduced from 19 to 7 pN, and a blockage is observed at an extension of about 50 bp, the position at which the G4 motif is expected. Once formed, without Pif1, the G4 structure does not unfold spontaneously during several hours, allowing enough time to test Pif1 activity on the G4 structure (Supplementary Figure S3). The force is then lowered to 4 pN in order to drive the full closure of the hairpin while encircling the G4 structure (step (5)). An illustration of our hairpin assay at the different extensions upon changes in the pulling force is shown in Figure 1A, right.

The dynamics of Pif1 unwinding was measured by tracking the position of the bead as described in (17). For this purpose, we developed a force protocol (Figure 1B- bottom panel) that allows visualizing different extensions of the hairpin in the presence of the G4 structure, as well as the interaction of the helicase with the structure. Once a G4 was folded, the force was kept at 11 pN and Pif1 was added to the microfluidic chamber at a concentration of 6 nM in the presence of 1 mM ATP. This force was chosen for two reasons, based on previous work by Li *et al.* (17): it is low enough to ensure that the hairpin remains closed, and it is high enough to increase the processivity of Pif1 larger than the size of our hairpin.

Pif1 resolves G4 structures but stalls transiently. In the absence of a preformed G4 structure, as observed by the total rezipping at 7 pN, (Figure 1B, blue, left panel), Pif1 binds to the single-stranded region of the closed hairpin (red arrow) and translocates along the lagging strand in the 5′-to-3′ direction. This results in the opening of the hairpin, which is detected by the extension of the molecule, and its subsequent rezipping once Pif1 has translocated past the hairpin loop and continues to translocate along the leading strand, which is seen by a decrease of extension at the same rate (see Supplementary Figure S4A). Alternatively, we also observed the spontaneous closing of the hairpin, which could correspond to either the dissociation of the helicase from the ssDNA, or its sliding back on the ssDNA (as exemplified in Figure 1B, blue, right panel).

In the presence of a preformed G4 structure on our first construct *LagG4* (Figure 1B, black, left panel), Pif1 binds to the hairpin (red arrow) and encounters the G4 structure during hairpin opening. The unwinding traces display a characteristic pause at the G4 position (Figure 1B, black, right panel at 3955 s and Figure 1C at 5704 s, see also Supplementary Figure S4B, C). After this pause, Pif1 resumes translocation all the way through the loop and along the leading strand, resulting in the closure of the hairpin behind the helicase. Furthermore, the absence of blockage during the rezipping of the hairpin confirms that the G4 structure was unfolded and did not reform after Pif1 translocated past it. Indeed, the absence of blockage is a signature of G4 resolving: a force of 11 pN is too high to allow the encirclement of the hairpin around a formed G4 structure (22); if the G4 structure were still present, the hairpin would not

close and we would observe a blockage at the same position as prior to Pif1 action. Another evidence for the resolution of G4 is that subsequent hairpin opening by Pif1 shows no pause at the G4 position, as observed in the first passage (Figure 1B, black curve, 3988 s, Supplementary Figure S5).

Figures 1C and D illustrate Pif1 unwinding the G4-containing hairpin substrate *LagG4*: first, the helicase attaches to the hairpin and translocates about 45 bases (step-(1)) before stalling at the level of the G4 (stalling position) for a varying period of time (ΔT_R^{LagG4}) (step-(2)). After resolving the G4, Pif1 resumes translocation all the way to the loop (step (3)) and onto the other strand, resulting in the full closing of the hairpin and dissociation of the helicase (step (4)). We measured the translocation speed along the lagging strand before (v_{unz1}) and after (v_{unz2}) Pif1 interacts with the G4, and found similar values of 108.4 ± 18.2 bp/s and 95.0 ± 20.1 bp/s respectively (Table 1 and Supplementary Methods).

Pif1 pausing times follow a single-exponential distribution (Figure 1E), with parameter $\tau_{LagG4} = 12.4 \pm 1.9$ s. τ_{LagG4} is much smaller than the spontaneous unfolding rate of the G4 at 11 pN in the absence of Pif1 ($\tau_{spontaneous} = 27400 \pm 6300$ s, see Supplementary Figure S3), which indicates that Pif1 catalyzes the unfolding of the G4 structure. Thus, we referred to the time spent by Pif1 at the G4 position as the G4 resolving time ΔT_R^{LagG4}. Figure 1F shows that while stalling (i.e. blockage at the G4 position) is observed during almost all unwinding events in the presence of a G4 structure (94%), it is almost never observed in the absence of a G4 structure (4% of unwinding events). Residual events can be attributed either to detection errors or to rare events of spontaneous folding/unfolding of G4 during the time elapsed between the detection cycle (Figure 1B, left) and the unwinding events (Figure 1B, right). Overall, our results confirm that Pif1 stalling is characteristic of the presence of a folded G4 structure. Our setup thus allows us to characterize the coupled dynamics of translocation and G4 interaction of Pif1. The observation of a pause in the presence of a G4 confirms previously published reports (33,34).

Pif1 switches strands and resumes translocation when stalled by a G4 in a geometry where the opposite strand is available

Another hairpin substrate geometry allows Pif1 to interact with the opposite strand. In the geometry of the previous assay (*LagG4*), the application of a force prevents the interaction of Pif1 with the opposite strand when it is stalled by the G4 structure (Figure 1D-step-(2)). Indeed, the G4 structure lies between the enzyme and the fork. Therefore, we designed a different hairpin substrate, referred to as *LeadG4*, in which the same G4 motif is located past the loop for a motor translocating in the 5′-to-3′ direction (Figure 2B and Supplementary Table S1). In this new configuration, Pif1 encounters the G4 structure after it translocated through the loop, and is located at the fork when it collides with the G4. Thus, we were able to study its interaction with a G4 structure in the vicinity of the opposite strand.

To form the G4, we used the same experimental protocol as the one used for *LagG4* assay. Figure 2A shows a representative trace of the dynamics of Pif1 during its interac-
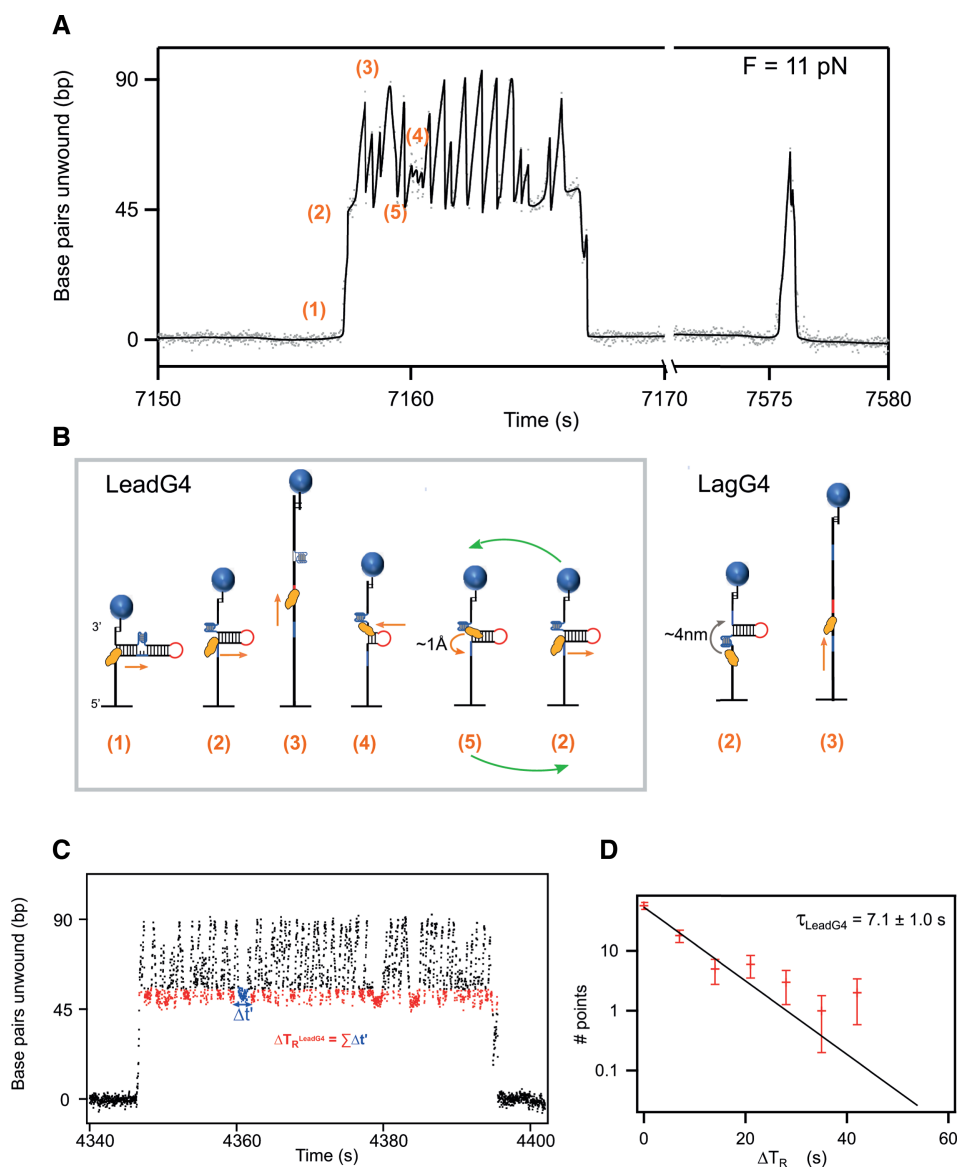
Figure 2. Pif1 activity on the LeadG4 hairpin. (**A**) Representative trace showing the collision of Pif1 when encountering a G4 while translocating through the hairpin. Various extensions of the hairpin are observed as Pif1 travels through it. Most relevant positions are indicated as orange numbers and described in the schematics in (**B**). Secondary opening of the hairpin by Pif1 at 7575 s shows no blockage. (**B**) Sketch of *LeadG4* hairpin. Left: In the *LeadG4* assay, Pif1 travels through the lagging strand (steps 1–3), passes the loop onto the leading strand (step 4), until it collides with G4 (step 5), the helicase manages to jump onto the other strand (a jump of ∼1 Å) and begins strand switching at the G4 position, visiting 5 and 2 repeatedly. Right: In the *LagG4* assay, strand switching at the G4 position is not favored, since the helicase would have to jump the whole structure (∼4 nm) to access the opposite strand. (**C**) Pif1 is stalled by a G4. The time Pif1 spends in contact with a G4 before strand switching (stalling time) is defined as $\Delta t'$ (example coloured in blue); the sum of all these individual times corresponds to the resolving time ΔT_R^{LeadG4} (all points in red). (**D**) Distribution of G4 resolving time in the *LeadG4* configuration at 6 nM of Pif1. The resolving times show a single exponential characterized by a time constant $\tau_{LeadG4} = 7.1 \pm 1.0$ s.

tion with the *LeadG4* substrate containing a G4 embedded within the hairpin, at the constant force of 11 pN. In this geometry, as expected, Pif1 translocates through the hairpin past the loop (Figure 2A, B-(steps (1) to (3)), onto the other strand causing the rezipping of the hairpin until it meets the G4 structure, (steps (4) and (5)).

G4 structure induces Pif1 strand switching. If Pif1 behaved in the same way in this new context, we would expect a single long pause at the G4 position during the rezipping of the hairpin. Then, Pif1 would resume translocation and the

hairpin would close completely. Interestingly, while we indeed observed a pause at the position of the G4 in the leading strand (stalling position, step-(5)), in most cases it was followed by an extension of the molecule, i.e. Pif1 resuming translocation back towards the loop (Figure 2A). As Pif1 translocation is directional, we interpreted this different behavior as Pif1 switching strand, allowed by the proximity of the complementary strand. Then, Pif1 resumes its translocation and passes the loop until it gets blocked again at the G4 position. This induces back and forth movements: the hairpin loop of our substrate confines the displacement of

the helicase, so that after switching direction at the G4 position, it finds itself again at the same position a few milliseconds later (Figure 2B, left steps (5) to (2), green arrow). In the *LagG4* assay, strand switching is not favored when Pif1 is at the G4 position (Figure 2B, right) because the opposite strand is further than a few (∼4 nm).

In Figure 2A, we observed a lower proportion of unfolding peaks with smaller extension (about 25%). This shows that Pif1 does not always reach the loop (as evidenced by a full extension of the hairpin), suggesting that it could strand switch (or detach) at any position in the lagging strand, as previously reported (17). Similarly, while Pif1 travels on the leading strand during refolding of the hairpin, it can strand switch before arriving to the G4 position (about 10% of the time). This is evidenced by smaller contractions. Strand switching thus depends on the context encountered by Pif1. Therefore, 90% of the strand switching events during refolding happen when Pif1 is blocked at the G4 position. We have therefore three independent but competing phenomena : strand switching present at any point where the complementary strand is in the vicinity, G4 resolution when Pif1 is in contact with the G4, and Pif1 detachment .These results actually imply that encountering G4 enhances Pif1 strand switching because it is blocked at a position with a nearby strand.

After repetitively unwinding and rewinding the hairpin, Pif1 finally goes through the G4 location and continues its translocation, resulting in the full closing of the hairpin (step (1)). We defined this behavior as a strand switching mechanism: Pif1 being stalled by the G4 structure can probabilistically switch to the opposite strand and resume translocation in the other direction. When Pif1 finally goes through the G4 position, we see again, as in the case of *LagG4*, that the G4 structure has been resolved, since the hairpin can fully close and does not exhibit the characteristic blockage at the G4 position. Furthermore, subsequent events generally do not show any more blockage (Figure 2A and Supplementary Figures S5 and S6).

We quantified the resolving time of the G4 by Pif1 with the *LeadG4* substrate, ΔT_R^{LeadG4}, as the total time spent by Pif1 in contact with the G4 before it resolves the secondary structure (sum of all red times shown in Figure 2C). Here again, ΔT_R^{LeadG4} follows a single-exponential distribution characterized by a time constant $\tau_{\text{LeadG4}} = 7.1 \pm 1.0$ s (Figure 2D). While it is not obvious why τ_{LeadG4} is half of τ_{LagG4}, this decrease of τ is not surprising, given the difference of geometry. Indeed, in this case, the fork rezips behind Pif1. This might favor its translocation ahead compared to the other geometry, where Pif1 is unwinding the hairpin during G4 resolution.

Individual stalling times ($\Delta t'$, in blue in Figure 2C), also follow a single-exponential distribution (Figure 3C, black) of parameter $\tau'_{\text{G4}} = 0.57 \pm 0.04$ s. This time is representative of the probability to switch strands.

In addition, we measured both the unzipping and rezipping velocities during strand switching transitions, and obtained very similar values within one standard deviation, of $v_{unz} = 94.6 \pm 10.0$ bp/s and $vz = 113.1 \pm 16.1$ bp/s. Hence, our results prove that both events are the result of the same helicase process (Table 1 and Supplementary Methods). Moreover, to test the ATP dependency of the

rate of DNA translocation, we carried out experiments at a lower concentration of ATP (50 μM, Supplementary Figure S7). While we observed the same strand switching mechanism, we measured a decrease in the average translocation speed from 95 bp/s to 71 bp/s, as expected (17). We showed again that translocation is constant along the lagging and leading strand, i.e. during unzipping or rezipping. The data for both rates at the concentrations of 1 mM and 50 μM of ATP are summarized in Supplementary Figure S7C.

Pif1 exhibits strand switching with obstacles other than G4

Visualization Pif1 colliding with heteroduplexes. To check whether the strand switching mechanism observed in the previous section is induced by a specific interaction with a G4, we replaced the G4 obstacle by RNA:DNA and LNA:DNA heteroduplexes localized at the same position in the sequence as the G4 motif in the leading strand configuration (Supplementary Figures S8 and S9). Here, to avoid the formation of the G4 structure, the 7 bp oligonucleotide (Oli7, see Material and Methods) was not injected into the microfluidic chamber during the experiment. Instead, we introduced 100 nM of a 34 bp LNA or RNA oligonucleotide complementary to the G4 sequence motif (Supplementary Table S1) and applied opening and closing cycles. The hybridization of the oligonucleotide to the hairpin can be detected by the blockage of the hairpin at the same position as the blockage induced by the G4 (Figure 3A, B).

LNA:DNA and RNA:DNA heteroduplexes also induce Pif1 strand switching. Once the LNA or RNA oligonucleotides were hybridized to the hairpin, we monitored Pif1 translocation as described above. As shown in Figures 3A and B, Pif1 translocation traces also display a strand switching behaviour when Pif1 reaches the heteroduplexes. After several back and forth events, Pif1 removes the LNA or RNA oligonucleotides and resumes translocation, as indicated by the full rezipping of the hairpin.

In the case of the LNA:DNA heteroduplex, some pauses in the back and forth mechanisms are observed before the removal of the oligonucleotide (Figure 3A). We interpreted these pauses as the waiting time between the unbinding of the helicase from the hairpin that did not manage to remove the obstacle and the binding of another helicase. Indeed, these pauses become shorter when the enzyme concentration in solution is increased by a factor 10 (as seen in Supplementary Figures S12A, B). In the case of RNA:DNA hybrid (Figure 3B), Pif1 manages to remove the RNA oligonucleotide 94% of the time before unbinding. This is not surprising considering that Pif1 processivity is enhanced on RNA:DNA substrate, and hence it preferentially translocates through the DNA strand while displacing the RNA strand (14,16). The resolution times were also computed as the average of the contact times of Pif1 with the heteroduplexes before their removal. We found $\overline{T}_{\text{LNA}} = 31.04 \pm 0.38$ s and $\overline{T}_{\text{RNA}} = 2.62 \pm 0.74$ s. The high resolving rate $k_{\text{RNA}} = \frac{1}{\overline{T}_{\text{RNA}}}$ compared to the one for G4 and LNA corroborates previous results pointing the efficiency of Pif1 for unwinding RNA:DNA hybrids.

Thanks to the spatial resolution of the experimental setup, it was possible to determine that strand switching and
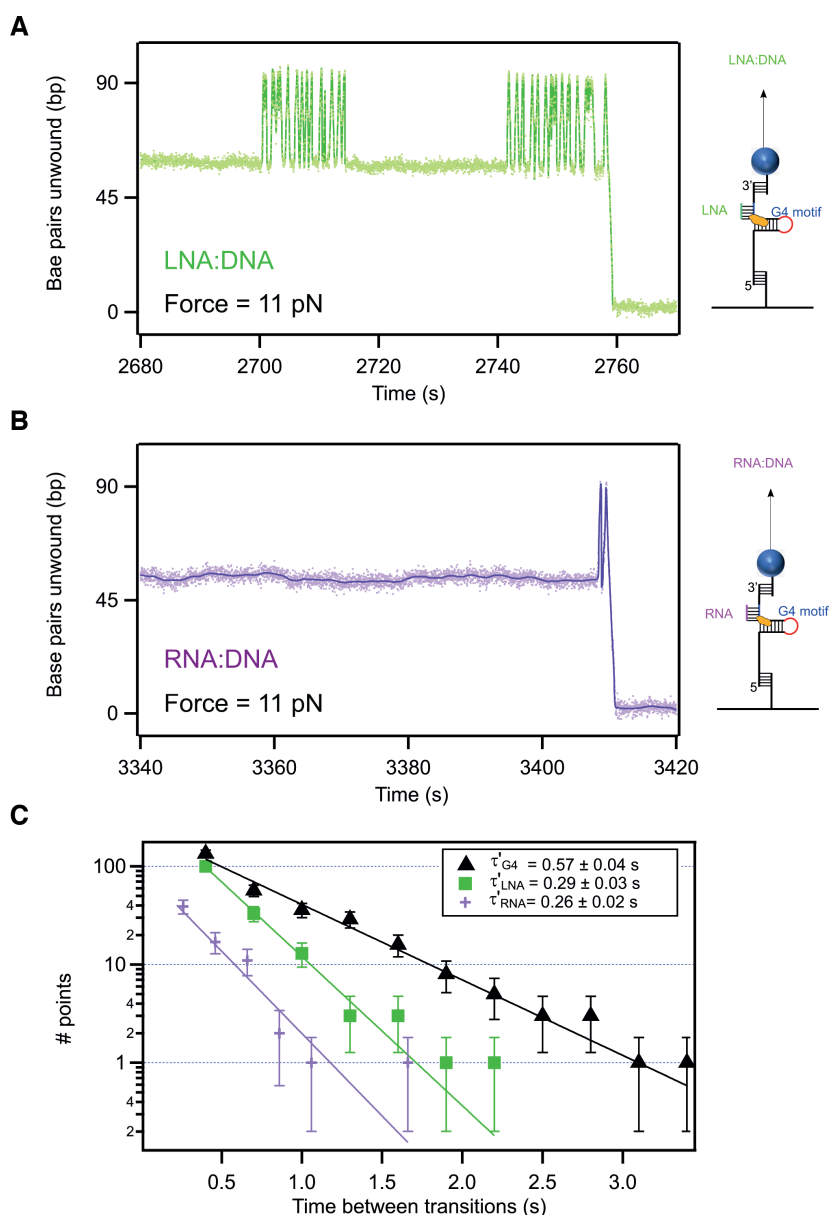
Figure 3. Pif1 translocating through LNA:DNA and RNA:DNA heteroduplexes. (**A**) Strand switching of Pif1 stimulated by a LNA:DNA heteroduplex. Representative trace of hairpin extension in the presence of Pif1 and a LNA:DNA heteroduplex. (**B**) Strand switching of Pif1 stimulated by a RNA:DNA heteroduplex. Representative trace of hairpin extension in the presence of Pif1 and a RNA:DNA heteroduplex. (**C**) Stalling time $\Delta t'$ for different obstacles: G4, LNA or RNA. The data correspond to the frequency of events in log scale *vs* time-between-transitions $\Delta t'$. The probability rate obeys a single exponential distribution with a time constant $\tau'_{LNA} = 0.29 \pm 0.03$ s (green), $\tau'_{RNA} = 0.26 \pm 0.02$ s (purple) and $\tau'_{G4} = 0.57 \pm 0.04$ s (black) for LNA, RNA and G4 respectively. In the G4 case, $\Delta t'$ includes all times measured at 6 and 60 nM, since differences between the resolving times obtained with the two concentrations were not significant (see Supplementary Figure S11).

stalling occur at the start of the heteroduplex and not on further positions along the hairpin. The stalling position for all our substrates was detected at around 50 opened base pairs, with a resolution of 5 bases (see Table 1-stalling position). This indicates that the limiting resolving step is the opening of the first bases of the heteroduplexes. Once the heteroduplexes are partially opened, Pif1 proceeds smoothly with their unwinding.

The probability to switch strands was quantified by the stalling times at the obstacle position (pause time between rezipping-unzipping events) as $\Delta t'$ as shown in Figure 3C (also Figure 2C-blue) . These times follow a single-exponential distribution of parameters $\tau'_{RNA} = 0.26 \pm 0.02$ s and $\tau'_{LNA} = 0.29 \pm 0.03$ s for RNA and LNA respectively, twice as small than G4 ($\tau'_{G4} = 0.57 \pm 0.03$ s).

In addition, we further verified the strand switching mechanism by measuring the interaction of Pif1 with another G4 structure containing the β^A-ori sequence in the *LeadG4* assay. Our measurements show that Pif1 also strand switches when encountering this structure, until resolving it in an average time of 2.7 s $\pm$ 3.3 s (Supplementary Figure S10).

Overall these results indicate that the strand switching mechanism of Pif1 is not specific to the c-MYC G4. When

Pif1 translocates along DNA and runs onto a G4 or a heteroduplex, the resolution of the obstacle is dictated by a competition between three dynamic processes: the resolution of the obstacle, the escape through strand switching and the unbinding of the enzyme.

DISCUSSION

In this work, we investigated the behavior of the *Saccharomyces cerevisiae* Pif1 helicase when it unwinds a DNA hairpin containing a G4 structure. We used methods developed in our previous study (22) to form and detect the G4 within a DNA hairpin, to study the behavior of Pif1 in the presence and absence of a G4. The setup allows us to visualize the translocation of the helicase along the dsDNA hairpin, its transient stalling at the position of the G4 in the sequence and the resolution of the structure. Our results show that Pif1 considerably shortens the G4 lifetime from hours to seconds (Supplementary Figure S3), confirming previous results showing that Pif1 actively promotes the unfolding of G4 structures and does not wait for the G4 to spontaneously unfold in order to resume translocation (16,18,33,34).

Two different substrates were used in this study: one in which the G4 motif is located on the translocation strand of Pif1 during unzipping (*LagG4*) and one in which the G4 motif is located on the translocation strand of Pif1 during the rezipping of the hairpin (*LeadG4*). The difference between these two substrates is that in one case (*LagG4*), the G4 is located between the helicase and the opposite strand, and therefore due to pulling at a constant force the other strand becomes hardly accessible. In the other configuration (*LeadG4*), Pif1 is lying between the opposite strand and the G4, making it very easy to switch to the other strand even under pulling conditions (Figure 2). For both substrates, Pif1 displays a pause when it meets the G4, quantitatively described in our assay by a stalling time $\Delta t'$, which follows a single exponential distribution. When the opposite strand is not available to the enzyme (*LagG4*), the traces display a unique stalling of typical time $\tau_{LagG4} \simeq 12$ s, followed by the resolution of the G4 secondary structure and resuming of translocation at the same speed (Figure 1). When the opposite strand is in close proximity to the enzyme (*LeadG4*), we observe a short stalling time of $\tau'_{G4} = 0.57$ s that is not sufficient to resolve the G4, and Pif1 readily switches translocating strands. However, in our hairpin configuration, the strand switching promotes further interactions with the G4 before the resolution of the G4 also takes place. The sum of all stalling times ΔT_R^{LeadG4}, during which Pif1 is close to the G4, also follows an exponential distribution of typical time $\tau_{LeadG4} \simeq 7$ s. Translocation speeds along both lagging and leading strand during strand switching are very similar as expected (Table 1), and decrease with lowering ATP (Supplementary Figure S7) in agreement with previous studies (17).

Our results therefore suggest that Pif1 can undergo two competitive mechanisms when it stalls at the G4 position. Either it switches strands and escapes the obstacle, with rate $k_{escape} = \frac{1}{\tau'_{G4}}$, or it catalyzes the G4 resolution when escape by strand switching is not available, and resumes translocation in the original direction with rate $k_{resolution} = \frac{1}{\tau_{LeadG4}}$.

In our case, k_{escape} is 12 times larger than $k_{resolution}$ and Pif1 switches strands most of the time. Due to the presence of the loop in the substrates, which confines the geometry of the DNA substrate, Pif1 stalls again at the G4 position a few seconds later and so on until it unfolds the G4. It is noteworthy that in the absence of a pulling force, Pif1 exhibits very low processivity that results in partial unwinding events that may not allow it to strand switch, as discussed in (21).

In previous single-molecule FRET experiments with a substrate mimicking a replication fork with a G-quadruplex on a free 5′ single-stranded flap (18), Zhang *et al.* observed a pause at intermediate FRET-levels between the binding of Pif1 to the fork and the subsequent unwinding of the duplex. They showed that the duration of this pause, which they called the 'waiting time', was inversely proportional to the concentration of Pif1 and thus suggested a mechanism where Pif1 is in a monomeric state when it solves the G4 and then must wait to be dimerized to perform the unwinding of the duplex. This model was supported by bulk experiments showing that Pif1 was able to dimerize on DNA substrates short as 5 bases (35). In our case, however, the resolving time did not significantly change when we increased the injected enzyme concentration from 6 nM to 60 nM (Supplementary Figures S11 and S12, and Table 1). Although our experiments do not allow controlling precisely the local enzyme concentration close to the DNA-coated surface nor to test the dimerization state of Pif1, they suggest that our resolving time is not equivalent to the waiting time observed in their studies. On the other hand, it is noteworthy that we observe the same translocation velocity of Pif1 before and after the collision and the resolution of the G4 (see Table 1), which points towards Pif1 being in the same oligomeric state, whether a monomer or a dimer. Finally, the dimer/monomer transition between translocating/G4 resolving Pif1 seems to fail to account for the strand switching behavior. If the pause between two translocation events corresponded to the time needed to bind to a second Pif1 partner, it is difficult to understand why it would be almost two orders of magnitudes lower in the case of the *LeadG4* substrate (0.57 s) with respect to the *LagG4* substrate (12 s). In our model, we understand the successive short pause times of Pif1 on the *LeadG4* substrate as the result of the competition between resolving and escaping the G4 by strand switching, an interpretation that is supported by the fact that the resolving time for *LeadG4* (7 s) inferred in this framework is of the same order of magnitude as for the *LagG4* substrate. Overall, our results raise questions over the current model of dynamic dimerization of Pif1.

Zhou *et al.*, then Lu *et al.* (16,20), showed that the helicase could also display a patrolling behavior, where it translocates along the ssDNA while staying bound at its starting point, thus creating a ssDNA loop. In our experiments, differentiating between patrolling and standard translocation is possible by measuring extension changes upon unzipping and rezipping. Patrolling would result in an extension twice as short than the one expected from the conversion between hybridized bases to ssDNA (~1 nm/bp (35), Supplementary Figure S13). The distribution of extension changes during unzipping of the hairpin shows that no patrolling occurs in our experiments. One
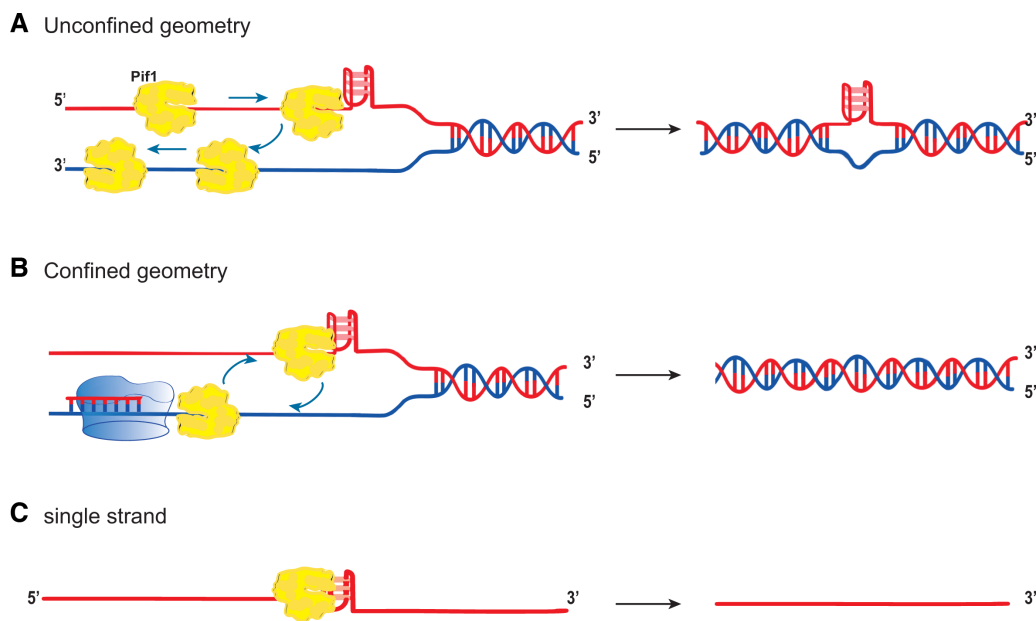
Figure 4. Could strand switching play a biological role? (**A**) Unconfined geometry. Pif1 switches strand and is able to escape through the other strand, avoiding obstacle resolution (**B**) Confined geometry. Pif1 is trapped within a fork and cycles around by strand switching, causing multiple collision with the G4 structure until G4 resolution. In this example, a hypothetical polymerase is shown as causing a confinement. (**C**) ssDNA configuration. Pif1 is unable to escape resolution, and resolves the G4 after a pause.

possible cause for our lack of observing patrolling is the small size of the ssDNA loading pad (7 bases in our experiment). Indeed, Lu *et al.* suggested that patrolling is due to a 'rare oligomeric form' of Pif1, which might need a longer pad to be able to bind to its substrate.

Another insight from our work is that Pif1 strand switching does not seem to be G4 specific, since we observed it also during the removal of RNA:DNA and LNA:DNA heteroduplexes on the translocation path of Pif1. In the case of RNA:DNA, our results confirm that the helicase removes this obstacle very easily. Interestingly, since Pif1 is not able to bind on a RNA strand (13), it may explain why the helicase exhibits higher processivity on RNA:DNA hybrids compared to dsDNA. The situation with RNA:DNA hybrids gives an indication of what happens with less stable G4, which are resolved after few strand switching events, and generally should not represent per se a major hindrance for the progression of molecular motors in the cell. In the case of dsDNA, the limited processivity of the enzyme would simply result from the competition between directional translocation on dsDNA and strand switching. In bulk experiments on longer DNA substrate, the low processivity of the enzyme might be due to sterile strand switching during dsDNA opening. The fact that Pif1 activity is enhanced by pulling of the hairpin in magnetic tweezers experiments argues in favor of this explanation (17). However, in the absence of tension, strand switching might be hindered by other Pif1 helicase behavior such as slippage-back. In this case, it would be observed as partial dsDNA unwinding, as previously reported in (21).

Overall, the single-molecule assay described here sheds new light on the behavior of Pif1. While previous work has shown the ability of Pif1 to remove roadblocks (12,15,36), competitive strand switching suggests refinement of its activity *in vivo*. Indeed, in the case of c-MYC-Pu27 studied

here, k_{escape} is 12 times larger than $k_{resolution}$. This means that Pif1 has 12 times more chances to switch strands than to resolve a stable G4 structure. Therefore, if the substrate was a long dsDNA substrate without a confining loop, as in the LeadG4 hairpin, Pif1 would escape the obstacle formed by G4-c-MYC-Pu27 with a probability of $\frac{k_{escape}}{k_{escape}+k_{resolution}} = 93\%$. As a consequence, this suggests a mechanism regarding the ability of Pif1 to remove G4 structures from its translocation path, unless it is confined and forced to repetitively enter in contact with the G4, for example by a polymerase or other larger molecular complexes, as sketched theoretically in Figure 4.

To conclude, Pif1 strand switching could be envisioned as a dual regulatory mechanism in vivo. It could prevent free Pif1 molecules from removing isolated secondary structures in the genome, while allowing G4 resolvase activity when Pif1 is confined in the context of a replisome, a R-loop (36), or acting on ssDNA overhangs at telomeres (11). This could explain the role of Pif1 in resolving G4 during active replication to ensure fidelity of DNA replication, without promoting G4-unfolding across the genome once the replication machinery has progressed through the structure. This activity would be compatible with epigenetic role previously suggested for G4 structures (37).

DATA AVAILABILITY

The datasets used in this study have been uploaded on Zenodo.org and can be retrieved at the following address: https://zenodo.org/record/6801824. Alternatively, they are available on request from the corresponding authors.

SUPPLEMENTARY DATA

Supplementary Data are available at NAR Online.

REFERENCES

1. Mendoza,O., Bourdoncle,A., Boulé,J.-B., Brosh,R.M. and Mergny,J.-L. (2016) G-quadruplexes and helicases. *Nucleic Acids Res.*, **44**, 1989–2006.
2. Spiegel,J., Adhikari,S. and Balasubramanian,S. (2020) The structure and function of DNA G-quadruplexes. *Trends Chem.*, **2**, 123–136.
3. Wickramasinghe,C.M., Arzouk,H., Frey,A., Maiter,A. and Sale,J.E. (2015) Contributions of the specialised DNA polymerases to replication of structured DNA. *DNA Repair.*, **29**, 83–90.
4. Bryan,T.M. (2019) Mechanisms of DNA replication and repair: insights from the study of G-quadruplexes. *Molecules*, **24**, 3439.
5. Varshney,D., Spiegel,J., Zyner,K., Tannahill,D. and Balasubramanian,S. (2020) The regulation and functions of DNA and RNA G-quadruplexes. *Nat. Rev. Mol. Cell. Biol.*, **21**, 459–474.
6. Linke,R., Limmer,M., Juranek,S.A., Heine,A. and Paeschke,K. (2021) The Relevance of G-Quadruplexes for DNA Repair. *Int. J. Mol. Sci.*, **22**, 12599.
7. Tarsounas,M. and Tijsterman,M. (2013) Genomes and G-quadruplexes: for better or for worse. *J. Mol. Biol.*, **425**, 4782–4789.
8. Bryan,T.M. (2020) G-quadruplexes at telomeres: friend or foe? *Molecules*, **25**, E3689.
9. Qi,T., Xu,Y., Zhou,T. and Gu,W. (2021) The evolution of G-quadruplex structure in mRNA untranslated region. *Evol. Bioinform. Online*, **17**, 11769343211035140.
10. Bohálová,N., Cantara,A., Bartas,M., Kaura,P., Šťastný,J., Pečinka,P., Fojta,M., Mergny,J.-L. and Brázda,V. (2021) Analyses of viral genomes for G-quadruplex forming sequences reveal their correlation with the type of infection. *Biochimie*, **186**, 13–27.
11. Muellner,J. and Schmidt,K.H. (2020) Yeast genome maintenance by the multifunctional PIF1 DNA helicase family. *Genes (Basel)*, **11**, E224.
12. Boulé,J.-B., Vega,L.R. and Zakian,V.A. (2005) The yeast Pif1p helicase removes telomerase from telomeric DNA. *Nature*, **438**, 57–61.
13. Boulé,J.-B. and Zakian,V.A. (2006) Roles of Pif1-like helicases in the maintenance of genomic stability. *Nucleic Acids Res.*, **34**, 4147–4153.
14. Boulé,J.-B. and Zakian,V.A. (2007) The yeast Pif1p DNA helicase preferentially unwinds RNA–DNA substrates. *Nucleic Acids Res.*, **35**, 5809–5818.
15. Koc,K.N., Singh,S.P., Stodola,J.L., Burgers,P.M. and Galletto,R. (2016) Pif1 removes a Rap1-dependent barrier to the strand displacement activity of DNA polymerase delta. *Nucleic Acids Res.*, **44**, 3811–3819.
16. Zhou,R., Zhang,J., Bochman,M.L., Zakian,V.A. and Ha,T. (2014) Periodic DNA patrolling underlies diverse functions of Pif1 on R-loops and G-rich DNA. *Elife*, **3**, e02190.
17. Li,J.-H., Lin,W.-X., Zhang,B., Nong,D.-G., Ju,H.-P., Ma,J.-B., Xu,C.-H., Ye,F.-F., Xi,X.G., Li,M. *et al.* (2016) Pif1 is a force-regulated helicase. *Nucleic Acids Res.*, **44**, 4330–4339.
18. Zhang,B., Wu,W.-Q., Liu,N.-N., Duan,X.-L., Li,M., Dou,S.-X., Hou,X.-M. and Xi,X.-G. (2016) G-quadruplex and G-rich sequence stimulate Pif1p-catalyzed downstream duplex DNA unwinding through reducing waiting time at ss/dsDNA junction. *Nucleic Acids Res.*, **44**, 8385–8394.
19. Barranco-Medina,S. and Galletto,R. (2010) DNA binding induces dimerization of *Saccharomyces cerevisiae* Pif1. *Biochemistry*, **49**, 8445–8454.
20. Lu,C., Le,S., Chen,J., Byrd,A.K., Rhodes,D., Raney,K.D. and Yan,J. (2019) Direct quantification of the translocation activities of *Saccharomyces cerevisiae* Pif1 helicase. *Nucleic Acids Res.*, **47**, 7494–7501.
21. Singh,S.P., Soranno,A., Sparks,M.A. and Galletto,R. (2019) Branched unwinding mechanism of the Pif1 family of DNA helicases. *Proc. Natl. Acad. Sci. U.S.A.*, **116**, 24533–24541.
22. Tran,P.L.T., Rieu,M., Hodeib,S, Joubert,A., Ouellet,J., Alberti,P., Bugaut,A, Allemand,J.-F., Boulé,J.-B. and Croquette,V. (2021) Folding and persistence times of intramolecular G-quadruplexes transiently embedded in a DNA duplex. *Nucleic Acids Res.*, **49**, 5189–5201.
23. Valton,A.-L., Hassan-Zadeh,V., Lema,I., Boggetto,N., Alberti,A., Saintomé,R.J.-F. and Prioleau,M.-N. (2014) G4 motifs affect origin positioning and efficiency in two vertebrate replicators. *EMBO J.*, **33**, 732–746.
24. Ruiz-Gutierreza,N., Rieu,M., Ouellet,J., Jean-François,A., Croquette,V. and Le Hir,H. (2022) Novel approaches to study helicases using magnetic tweezers. *Methods Enzymol.*, https://doi.org/10.1016/bs.mie.2022.03.035.
25. Gosse,C. and Croquette,V. (2002) Magnetic tweezers: micromanipulation and force measurement at the molecular level. *Biophys J*, **82**, 3314–3329.
26. Fiorini,F., Bagchi,D., Le Hir,H. and Croquette,V. (2015) Human Upf1 is a highly processive RNA helicase and translocase with RNP remodelling activities. *Nat. Commun.*, **6**, 7581.
27. Rieu,M., Vieille,T., Radou,G., Jeanneret,R., Ruiz-Gutierrez,N., Ducos,B., Allemand,J.-F. and Croquette,V. (2021) Parallel, linear, and subnanometric 3D tracking of microparticles with stereo darkfield interferometry. *Sci Adv*, **7**, eabe3902.
28. Kanaan,J., Raj,S., Decourty,L., Saveanu,C., Croquette,V. and Le Hir,H. (2022) Human Upf1 is a highly processive RNA helicase and translocase with RNP remodelling activities. *Nat Commun*, **9**, 3752.
29. Boulé,J.-B. and Zakian,V.A. (2010) Characterization of the helicase activity and anti-telomerase properties of yeast Pif1p in vitro. *Methods Mol Biol*, **587**, 359–376 .
30. Ribeyre,C., Lopes,J., Boulé,J.-B., Piazza,A., Guédin,A., Zakian,V.A., Mergny,J.-L. and Nicolas,A. (2009) The yeast Pif1 helicase prevents genomic instability caused by G-quadruplex-forming CEB1 sequences in vivo. *PLoS Genet.*, **5**, e1000475.
31. Chung,S.H. and Kennedy,R.A. (1991) Forward-backward non-linear filtering technique for extracting small biological signals from noise. *PLoS Genet.*, **40**, 71–86.
32. Gabelica,V., Shammel Baker,E., Teulade-Fichou,M.-P., De Pauw,E. and Bowers,M.T. (2007) Stabilization and structure of telomeric and c-myc region intramolecular G-quadruplexes: the role of central cations and small planar ligands. *J. Am. Chem. Soc.*, **129**, 895–904.
33. Wang,L., Wang,Q.-M., Wang,Y.-R., Xi,X.-G. and Hou,X.-M. (2018) DNA-unwinding activity of *Saccharomyces cerevisiae* Pif1 is modulated by thermal stability, folding conformation, and loop lengths of G-quadruplex DNA. *J. Biol. Chem.*, **293**, 18504–18513.
34. Byrd,A.K. and Raney,K.D. (2015) A parallel quadruplex DNA is bound tightly but unfolded slowly by Pif1 helicase. *J. Biol. Chem.*, **290**, 6482–6494.
35. Manosas,M., Spiering,M. M, Ding,F., Bensimon,D., Allemand,J.-F., Benkovic,S.J. and Croquette,V. (2012) Mechanism of strand displacement synthesis by DNA replicative polymerases. *Nucleic Acids Res.*, **40**, 6174–6186.
36. Schauer,G.D., Spenkelink,L.M., Lewis,J.S., Yurieva,O., Mueller,S.H., van Oijen,A.M. and O'Donnell,M.E.V. (2020) Replisome bypass of a protein-based R-loop block by Pif1. *Proc. Natl. Acad. Sci. U.S.A.*, **117**, 30354–30361.
37. Sarkies,P., Murat,P., Phillips,L.G., Patel,K.J., Balasubramanian,S. and Sale,J.E. (2012) FANCJ coordinates two pathways that maintain epigenetic stability at G-quadruplex DNA. *Nucleic Acids Res.*, **40**, 1485–1498.